Comparison of vibrational conductivity and radiative energy transfer methods

Alain Le Bot

Comparison of vibrational conductivity and radiative energy transfer methods

A. LE BOT
Laboratoire de Tribologie et Dynamique des Systèmes CNRS
École centrale de Lyon, FRANCE alain.le-bot@ec-lyon.fr

Abstract

This paper is concerned with the comparison of two methods well-suited for the prediction of the wideband response of built-up stuctures subjected to high frequency vibrational excitation. The first method is sometimes called the *vibrational conductivity method* and the second one is rather known as the *radiosity method* in the field of acoustics, or the *radiative energy transfer method*. Both are based on quite similar physical assumptions *i.e.* uncorrelated sources, mean response and high frequency excitation. Both are based on analogies with some equations encountered in the field of heat transfer. However these models do not lead to similar results. This paper compares the two methods. Some numerical simulations on a pair of plates joined along one edge are provided to illustrate the discussion.

1 Introduction

For many years, there have been attempts to generalize the Statistical Energy Analysis (SEA) in such a way that the repartition of energy inside sub-systems can be predicted. Among these attempts, the so-called *power flow finite element analysis* [1], *energy finite element method* [2] or *vibrational conductivity approach* [3] has been studied by several laboratories. This is a direct generalization of SEA for non diffuse fields. The flow of energy is assumed to be proportional to the difference of energy levels, as in SEA where the exchanged power is proportional to the difference of modal energies. But the relationship now is local, leading to an analogy with Fourier's law in heat conduction. The governing equation for energy density is thus quite similar to the conduction equation in heat transfer with a convective term. This analogy has been developed to allow the use of thermal software in order to solve some problems in structural vibrations [1, 4]. This method has been successfully applied to bars, beams [2, 5], membranes [6], plates [7, 8] and built-up structures [9].

In the field of acoustics, the so-called *radiosity method* [10, 11, 12, 13, 14] has been developed to allow the prediction of time reverberation in complex rooms beyond the validity of Sabine's formula. This method seems to stem from the field of radiative heat transfer and, more precisely, is analogous to the so-called *standard procedure* or *view factor method*. However, the aims of the radiosity method and the standard procedure are quite different, the prediction of reverberation time for the former and the prediction of the temperature of walls for the latter. More recently, these methods have been applied in structural acoustics [15, 16, 17, 18]. The resulting method is able to predict the decrease of energy, the time reverberation, but also the repartition of energy in

steady state conditions. Diffraction effects have also been included especially to take into account the radiation of sound by structures [19].

It is clear that the two methods, that is to say, the vibrational conductivity method on the one hand and the radiative energy transfer method on the other hand, apply for the calculation of the repartition of energy in built-up structures. Both methods are also based on analogies with some equations in thermics, conduction for the former and radiative heat transfer for the latter.

This paper aims to compare the results of these methods. The discussion is focused on a typical example, a pair of joined plates excited by out-of-plane motions. The paper is organized as follows. Section 2 introduces the basic concepts of the vibrational conductivity and section 3 introduces the radiative energy transfer. Some comments are given in Section 4. For the sake of simplicity, both methods are restricted to steady state vibration of a scalar wave field. In Section 5 , the solutions of the governing equations are presented for the joined plates and, finally, in Section 6, some numerical simulations are compared and discussed.

2 Vibrational conductivity

The vibrational conductivity is first based on the local energy balance in steady state condition,

$$div\mathbf{I} + \eta\omega W = \rho, \tag{1}$$

where $\mathbf{I}$ is the structural intensity vector, η is the damping loss factor, ω is the circular frequency, W is the energy density, $\eta\omega W$ is the power density being dissipated and ρ is the power density being injected. By integrating Eq. (1) overall the system Ω leads to

$$P_{\text{inj}} = \eta\omega W_{\Omega}, \tag{2}$$

where $P_{\text{inj}} = \int_{\Omega} \rho \mathrm{d}\Omega$ is the total injected power and $W_{\Omega} = \int_{\Omega} W \mathrm{d}\Omega$ is the total vibrational energy.

The most fundamental assumption of the vibrational conductivity is that the intensity can be related to the energy density with the relationship

$$\mathbf{I} = -\frac{c^2}{\eta\omega}\mathbf{grad}W, \tag{3}$$

where c is the group speed. This equation is well verified for a plane wave travelling in a damped medium and also for a superposition of uncorrelated plane waves [6, 7]. By introducing Eq. (3) into Eq. (1), it yields

$$-\frac{c^2}{\eta\omega}\Delta W + \eta\omega W = \rho. \tag{4}$$

This is a second order partial differential equation which is analogous to the conduction equation in heat transfer with a convective term. This equation can be solved with the finite element method although it is also possible to re-use the numerous thermic softwares.

Several types of boundary conditions can be applied. The simplest one is obtained by considering that the net outgoing power density $P = \mathbf{I}.\mathbf{n} = -c^2/\eta\omega \times \partial W/\partial \mathbf{n}$ where $\mathbf{n}$ is the unit normal to the boundary, is zero on the boundary *i.e* the boundary is conservative,

$$P = 0. \tag{5}$$

At the common edge of two structures such as bars, beams, membranes or plates, the coupling conditions usually encountered in the literature involve the averaged transmission and reflection efficiencies $\bar{\tau}_{ij} = \int_0^{\pi/2} \tau_{ij}(\theta) \cos\theta \mathrm{d}\theta$ where $\tau_{ij}(\theta)$ is defined as the ratio of the power transmitted towards sub-system j over the power coming from sub-system i at incidence θ. For a non-dissipating interface, $\sum_j \bar{\tau}_{ij} = 1$. If the right-travelling power in the sub-structure i is denoted by P_i^+ with $i = 1, 2$ and the left-travelling power is denoted by P_i^-, the coupling conditions are

$$P_1^- = \bar{\tau}_{11} P_1^+ + \bar{\tau}_{21} P_2^-, \tag{6}$$

$$P_2^+ = \bar{\tau}_{12} P_1^+ + \bar{\tau}_{22} P_2^-, \tag{7}$$

the sub-structure 1 being on the left side. Eqs. (6) and (7) have been introduced in Ref. [5] for coupled beams where the wave decomposition (left- and right-travelling waves) is straightforward. The same conditions are used for coupled plates in Ref. [8] where Eq. (4) is solved using a wave decomposition which allows to clearly separate the left- and right-travelling powers. A slightly different approach is adopted in Ref. [9]. The total energy is the sum of left- and right-travelling energies, $W_i = W_i^+ + W_i^-$, and similarly, $P_i = P_i^+ - P_i^-$. Defining the mean speed of incidence of energy v_i as the ratio of power over energy, $P_i^+ = v_i W_i^+$ and $P_i^- = v_i W_i^-$, the left- and right-travelling powers are related to total quantities with, $2P_i^+ = v_i W_i + P_i$ and $2P_i^- = v_i W_i - P_i$. By subtituting these relationships into Eqs. (6) and (7), it yields

$$P_1 = \frac{\pi}{2} \left(\mu_1 v_1 W_1 - \mu_2 v_2 W_2 \right), \tag{8}$$

$$P_2 = \frac{\pi}{2} \left(\mu_1 v_1 W_1 - \mu_2 v_2 W_2 \right). \tag{9}$$

where $\mu_1 = \bar{\tau}_{12}/\pi\bar{\tau}_{11}$ and $\mu_2 = \bar{\tau}_{21}/\pi\bar{\tau}_{22}$. Note that in general $\mu_1 \neq \mu_2$. In Eqs. (8), (9) and all subsequent ones, powers are positive if energy flows from left to right and thus, $P_i = -c_i^2/\eta\omega \times \partial W_i/\partial \mathbf{n}$ where $\mathbf{n}$ is the unit normal to the interface oriented from sub-structure 1 to sub-structure 2. Equality of net powers P_1 and P_2 is clear from Eqs. (8) and (9). Eqs. (6) and (7) and Eqs. (8) and (9) are equivalent provided that a correct expression for the mean speed of incidence of energy is used. Assuming that the field is diffuse in the vicinity of the interface, all incidences are equiprobable. Then, the mean value for the velocity normal to the interface of plane waves is

$$v = c\frac{2}{\pi} \int_0^{\pi/2} \cos\theta \mathrm{d}\theta = \frac{2}{\pi} c. \tag{10}$$

Furthermore, the assumption of light coupling $\bar{\tau}_{12}, \bar{\tau}_{21} << 1$, is usually done, although it seems to be not necessary, leading to $\mu_1 = \bar{\tau}_{12}/\pi$ and $\mu_2 = \bar{\tau}_{21}/\pi$. Thus, the coupling conditions for the interface are

$$P_1 = \frac{1}{\pi} \left(\bar{\tau}_{12} c_1 W_1 - \bar{\tau}_{21} c_2 W_2 \right), \tag{11}$$

$$P_2 = \frac{1}{\pi} \left(\bar{\tau}_{12} c_1 W_1 - \bar{\tau}_{21} c_2 W_2 \right). \tag{12}$$

Let compare Eqs. (11) and (12) with the classical SEA equation,

$$\mathcal{P}_{12} = \omega \left(\eta_{12} W_{\Omega_1} - \eta_{21} W_{\Omega_2} \right), \tag{13}$$

where $\mathcal{P}_{12}$ is the exchanged power from sub-system 1 to sub-system 2 and W_Ω is the total vibrational energy of system Ω. For a diffuse field $W_{\Omega_i} = W_i S_i$ where S_i is the area of sub-system i and $\mathcal{P}_{12} = P_1 b$ where b is the length of the common edge. It is then apparent that Eqs. (11) and (12) leads to the coupling loss factors,

$$\eta_{ij} = \frac{b c_i}{\pi \omega S_i} \bar{\tau}_{ij}, \tag{14}$$

which is consistent with the classical wave approach of SEA [20, 21]. The coupling conditions (11) and (12) were first derived in Ref. [3] where the link with SEA is also remarked.

3 Radiative energy transfer

In the radiative energy transfer, the energy density at any point $\mathbf{r}$ in the domain Ω is given by superimposing the contributions of actual sources of power density ρ and fictitious sources of power density σ/π located on the boundary Γ which reflects the energy,

$$W(\mathbf{r}) = \int_\Omega \rho(\mathbf{s}) \frac{\mathrm{e}^{-mR}}{2\pi cR} \mathrm{d}\Omega_\mathbf{s} + \int_\Gamma \sigma(\mathbf{q}) \cos\theta \frac{\mathrm{e}^{-mR'}}{2\pi cR'} \mathrm{d}\Gamma_\mathbf{q}, \tag{15}$$

where $R = |\mathbf{r}-\mathbf{s}|$, $R' = |\mathbf{r}-\mathbf{q}|$, θ is the emission angle at point $\mathbf{q}$ *i.e.* the angle between the normal $\mathbf{n}$ and the direction $\mathbf{r}-\mathbf{q}$. $\mathrm{e}^{-mR}/2\pi cR$ is the contribution of a unit source at a distance R for two-dimensional systems such as plates, with m being the absorption factor. A similar expression for the intensity is

$$\mathbf{I}(\mathbf{r}) = \int_\Omega \rho(\mathbf{s}) \frac{\mathrm{e}^{-mR}}{2\pi R} \mathbf{u} \mathrm{d}\Omega_\mathbf{s} + \int_\Gamma \sigma(\mathbf{q}) \cos\theta \frac{\mathrm{e}^{-mR'}}{2\pi R'} \mathbf{u}' \mathrm{d}\Gamma_\mathbf{q}, \tag{16}$$

where $\mathbf{u} = (\mathbf{r}-\mathbf{s})/R$ and $\mathbf{u}' = (\mathbf{r}-\mathbf{q})/R'$. This equation is valid for any $\mathbf{r}$ lying inside the domain Ω. A similar equation is obtained for any point $\mathbf{p}$ belonging to the boundary Γ by taking the limit $\mathbf{r} \to \mathbf{p} \in \Gamma$. It results in [22],

$$\mathbf{I}(\mathbf{p}) = \int_\Omega \rho(\mathbf{s}) \frac{\mathrm{e}^{-mR}}{2\pi R} \mathbf{u} \mathrm{d}\Omega_\mathbf{s} + \int_\Gamma \sigma(\mathbf{q}) \cos\theta \frac{\mathrm{e}^{-mR'}}{2\pi R'} \mathbf{u}' \mathrm{d}\Gamma_\mathbf{q} - \frac{\sigma(\mathbf{p})}{\pi} \mathbf{n}, \tag{17}$$

where $\mathbf{n}$ is the outward unit normal to the boundary at point $\mathbf{p}$.

The function $G(R) = \mathrm{e}^{-mR}/2\pi cR$ appearing in Eqs. (15)-(17) may be justified as follows. This is the energy field which results from a unique driving point with unit power in an unbounded domain Ω. This can be checked by substituting $\rho = \delta$ in Eq. (15) and by cancelling the second integral. In another hand, it is shown in Appendix A that this function arises from the integral form solution of Love plate equation when assessing the energy density under the assumption that all waves are uncorrelated. Monopoles, dipoles and other multipoles radiate energy following the same $\mathrm{e}^{-mR}/2\pi cR$ law but with different directivities. A further argument in favour of this law is that the energy field $G(R)$ jointly with the intensity field $H(R) = cG(R)$, verify the power balance [16],

$$div\mathbf{H} + mcG = \delta. \tag{18}$$

Any other choice for G and $\mathbf{H}$ would violate the power balance.

In the second integrals of Eqs. (15)-(17), a cosine law is employed for the directivity of reflective sources $\sigma(\mathbf{p})$. This is Lambert's law. In Appendix A, it is shown that the boundary reflects energy with a directivity which is not the same for every points, that is $\sigma(\mathbf{p}, \theta)$ depends on the position $\mathbf{p}$ and also on the emanating angle θ. A statistical law can be adopted if rays, after several reflections, forgot their initial direction. This property, called "mixing" in billiards theory, arises for systems with complex geometries. Then it is well-known [23] that the only permissible memoryless law for reflectivity, that is a law identical everywhere and which does not depend on incident direction, is the cosine Lambert's law.

These fields W and $\mathbf{I}$ verify the local power balance in steady state condition,

$$div\mathbf{I} + mcW = \rho, \tag{19}$$

which is, indeed, similar to Eq. (1) provided that $m = \eta\omega/c$. The global power balance is

$$P_{\text{inj}} = mcW_\Omega, \tag{20}$$

with same notations as in Eq. (2).

The power of actual sources is assumed to be known. But the power reflected by the boundary is an unknown. The equation on σ is derived by applying the condition $\mathbf{I}.\mathbf{n} = 0$ at any point $\mathbf{p}$ of the boundary,

$$\frac{1}{\pi}\sigma(\mathbf{p}) = \int_\Omega \rho(\mathbf{s})\frac{\mathrm{e}^{-mR}}{2\pi R}\cos\varphi \mathrm{d}\Omega_\mathbf{s} + \int_\Gamma \sigma(\mathbf{q})\cos\theta\frac{\mathrm{e}^{-mR'}}{2\pi R'}\cos\varphi \mathrm{d}\Gamma_\mathbf{q}, \tag{21}$$

where φ is the incidence angle at point $\mathbf{p}$. The left hand-side is the reflected power whereas the right hand-side is the incident power, the first integral being the power supplied by actual sources and the second integral being the power supplied by other fictitious sources. This is a Fredholm integral equation of second kind valid for non absorbing boundaries. More elaborated equations can be derived for absorbing boundaries [10] and for diffusely or specularly reflecting boundary [22].

Finally, the coupling conditions on the unknowns σ_i at interfaces of two sub-systems $i = 1, 2$ are [16, 17]

$$\frac{1}{\pi}\sigma_i(\mathbf{p}) = \sum_j \int_{\Omega_j} \tau_{ji}(\varphi)\rho_j(\mathbf{s})\frac{\mathrm{e}^{-m_j R}}{2\pi R}\cos\varphi \mathrm{d}\Omega_\mathbf{s} + \int_{\Gamma_j} \tau_{ji}(\varphi)\sigma_j(\mathbf{q})\cos\theta\frac{\mathrm{e}^{-m_j R'}}{2\pi R'}\cos\varphi \mathrm{d}\Gamma_\mathbf{q}, \tag{22}$$

where the sum in the right hand-side runs over $j = 1, 2$. Eq. (22) involves the transmission efficiencies $\tau_{ij}(\varphi)$ at incidence φ and not the mean efficiencies $\bar{\tau}_{ij}$.

4 Comments

The fundamental solution of Eq. (4) is $g(R) = \eta\omega/2\pi c^2 \times \mathrm{K}_0(mR)$ where K_0 is the modified Bessel function of second kind and order zero and $m = \eta\omega/c$. The differential equation (4) is then equivalent to the integral equation,

$$W(\mathbf{r}) = \int_\Omega \rho(\mathbf{s})g(R)\mathrm{d}\Omega_\mathbf{s} + \frac{c^2}{\eta\omega}\int_\Gamma \frac{\partial W}{\partial n}(\mathbf{q})g(R') - W(\mathbf{q})\frac{\partial g}{\partial n}(R')\mathrm{d}\Gamma_\mathbf{q}, \tag{23}$$

which reads,

$$W(\mathbf{r}) = \frac{\eta\omega}{2\pi c^2} \times \left(\int_\Omega \rho(\mathbf{s})\mathrm{K}_0(mR)\mathrm{d}\Omega_\mathbf{s} + \int_\Gamma cW(\mathbf{q})\cos\theta\mathrm{K}_1(mR') - P(\mathbf{q})\mathrm{K}_0(mR')\mathrm{d}\Gamma_\mathbf{q}\right), \tag{24}$$

where P is the net outgoing power. This equation is to be compared with Eq. (15) for the radiative energy transfer. However, it appears several differences. First of all, an asymptotic development of g in far-field is $g(R) = (m/8\pi c^2)^{1/2} \times \mathrm{e}^{-mR}/\sqrt{R}$ showing that the decrease is like $1/\sqrt{R}$, unlike

$1/R$ for radiative transfer. Furthermore, in near-field $g(R) = -m/2\pi c \times \log mR$, unlike $1/R$ for radiative transfer. Thus, $G > g$ when $mR << 1$ and $G < g$ when $mR >> 1$. Secondly, Eq. (24) involves two layers whereas Eq. (15) just has a single layer. However, for large arguments $\mathrm{K}_0(z) = \mathrm{K}_1(z) = \mathrm{e}^{-z}\sqrt{\pi/2z}$ and then for $\mathbf{r}$ being far from the boundary $mR' >> 1$ it yields,

$$W(\mathbf{r}) = \int_\Omega \rho(\mathbf{s})\sqrt{\frac{m}{8\pi}}\frac{\mathrm{e}^{-mR}}{c\sqrt{R}}\mathrm{d}\Omega_\mathbf{s} + \int_\Gamma [cW(\mathbf{q})\cos\theta - P(\mathbf{q})]\sqrt{\frac{m}{8\pi}}\frac{\mathrm{e}^{-mR'}}{c\sqrt{R'}}\mathrm{d}\Gamma_\mathbf{q}. \tag{25}$$

Thus, both methods leads to the conclusion that a single layer is enough to describe the energy in far-field. In addition, when $P = 0$ (on the edges of plates), the magnitude of the boundary source in Eq. (25) is $cW(\mathbf{q})\cos\theta$ showing that, in accordance with the radiative transfer approach, the directivity follows Lambert's law. The only disagreement between both methods is then the choice of the direct field, g or G.

It now arises the question of whether the energy field given in Eq. (15) can be solution of a differential equation. As superposition applies to energy field (under the assumption that interferences have been neglected), the differential operator must be linear. Furthermore, considering plane plates, the differential operator must respect homogeneity and isotropy of space. Homogeneity implies that coefficients of the operator are constant and isotropy leads to further conditions. It is straighforward by a direct calculation that, up to the order 2, the only differential operators with constant coefficients obeying isotropy are identity, Laplacian and, indeed, any linear combinations of the two. It is now apparent that G cannot be the fundamental solution of these operators. In Appendix C, it is shown that this conclusion is valid for any order in dimension 2 and, thus the field given in Eq. (15) cannot be obtained by solving a differential problem.

5 Solutions for a pair of plates

Let consider a pair of rectangular plates of length a and width b and joined along a common edge as shown in Fig. 1. The plates are in the same plane with simply supported edges excepted the common edge which is free. The plates are made of the same material with different thicknesses. The plates are excited by some transverse forces located at x_s, y_s, $s = 1, 2, ...$ in a local frame whose origin is the lower left corner of the plate (Fig. 1). The density of power being injected of Eqs. (4) and (15) is thus, $\rho(x, y) = \sum_s P_s\delta(x - x_s)\delta(y - y_s)$ where P_s is the power injected by the s^{th} force.

The solution for the vibrational conductivity equation (4) is expanded as a Fourier series,

$$W(x, y) = \sum_{n=0}^{\infty} W_n(x)\cos(\frac{n\pi y}{b}), \tag{26}$$

where the sine functions has been discarded since the condition $\partial W/\partial y = 0$ applies at $y = 0$ and $y = b$. Substitution of Eq. (26) into Eq. (4) yields

$$\frac{\mathrm{d}^2 W_n}{\mathrm{d}x^2} - \left[(\frac{n\pi}{b})^2 + (\frac{\eta\omega}{c})^2\right] W_n = -\frac{2 - \delta_n}{b}\frac{\eta\omega}{c^2}\sum_s P_s\cos(\frac{n\pi y_s}{b})\delta(x - x_s), \tag{27}$$

where $\delta_n = 1$ if $n = 0$ and $\delta_n = 0$ otherwise. The general solution for this differential equation is,

$$W_n(x) = A_n\mathrm{e}^{-\alpha_n x} + B_n\mathrm{e}^{-\alpha_n(a-x)} + \sum_s C_{ns}\mathrm{e}^{-\alpha_n|x_s - x|}, \tag{28}$$

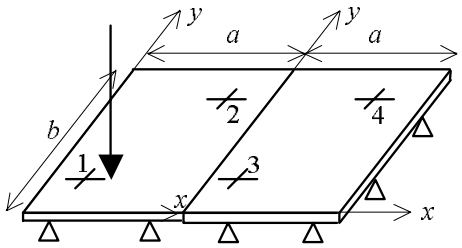

Figure 1: Two coplanar plates with different thicknesses. The edges are simply supported excepted the common edge which is free. The first plate is excited by a transverse force and four receiver points are located on both plates.

where

$$\alpha_n = \left[(\frac{n\pi}{b})^2 + (\frac{\eta\omega}{c})^2 \right]^{1/2}, \tag{29}$$

and

$$C_{ns} = P_s \frac{2-\delta_n}{2b\alpha_n} \times \frac{\eta\omega}{c^2} \cos(\frac{n\pi y_s}{b}). \tag{30}$$

The right hand-side of Eq. (28) may be splitted into two terms, one term W^+ is attached to the right-travelling wave and the other one W^- to the left-travelling wave,

$$W_n^+(x) = A_n \mathrm{e}^{-\alpha_n x} + \sum_s C_{ns} \mathrm{Y}(x - x_s) \mathrm{e}^{-\alpha_n |x_s - x|}, \tag{31}$$

$$W_n^-(x) = B_n \mathrm{e}^{-\alpha_n (a-x)} + \sum_s C_{ns} \mathrm{Y}(x_s - x) \mathrm{e}^{-\alpha_n |x_s - x|}, \tag{32}$$

where Y is the Heaviside function. The powers flowing in x-direction are derived by applying Eq. (3),

$$P_n^+(x) = \frac{\alpha_n c^2}{\eta\omega} \left[A_n \mathrm{e}^{-\alpha_n x} + \sum_s C_{ns} \mathrm{Y}(x - x_s) \mathrm{e}^{-\alpha_n |x_s - x|} \right], \tag{33}$$

$$P_n^-(x) = \frac{\alpha_n c^2}{\eta\omega} \left[B_n \mathrm{e}^{-\alpha_n (a-x)} + \sum_s C_{ns} \mathrm{Y}(x_s - x) \mathrm{e}^{-\alpha_n |x_s - x|} \right]. \tag{34}$$

Inside each plate $i = 1, 2$, the total energy densities, left- and right-travelling energies and left- and right-travelling powers are given by Eqs. (28)-(34). The speed of incidence of energy for the n^{th} component is

$$v_n = \frac{\alpha_n c^2}{\eta\omega}. \tag{35}$$

In Ref. [8], the coupling conditions (6) and (7) are applied with the left- and right-travelling powers given in Eqs. (33) and (34). Thus, the actual speed of energy given in Eq. (35) is employed for the n^{th} component, instead of the mean speed appearing in Eqs. (11) and (12). In a similar manner, it is possible to substitute in Eqs. (8) and (9) the efficiencies τ_{ij} at the incidence of the n^{th} component instead of the mean efficiencies $\bar{\tau}_{ij}$ valid for diffuse incidence. However, this approach

requires the knowledge of each component and then, deeply depends on the cosine development (26) adopted for the solution of Eq. (4). It seems to be limited to the particular case of a line of plates. The approach of Refs. [3, 9] is adopted in this paper, with the mean speed of incidence given in Eq. (10) and the efficiencies $\bar{\tau}_{ij}$ averaged over all incidences.

The constants $A_{i,n}$ and $B_{i,n}$ attached to the plate i are determined by applying Eqs. (5), (11) and (12). The boundary conditions (5) are $P_{1,n}(0) = 0$ and $P_{2,n}(a) = 0$ and the coupling conditions (11) and (12) at the interface are, $P_{1,n}(a) = P_{2,n}(0) = \bar{\tau}_{12}c_1/\pi W_{1,n}(a) - \bar{\tau}_{21}c_2/\pi W_{2,n}(0)$. All these conditions are summarized in the system

$$\begin{pmatrix} 1 & -\mathrm{e}^{-\alpha_{1,n}a} & 0 & 0 \\ (v_{1,n}-\mu_1 c_1)\mathrm{e}^{-\alpha_{1,n}a} & -v_{1,n}-\mu_1 c_1 & \mu_2 c_2 & \mu_2 c_2 \mathrm{e}^{-\alpha_{2,n}a} \\ -\mu_1 c_1 \mathrm{e}^{-\alpha_{1,n}a} & -\mu_1 c_1 & v_{2,n}+\mu_2 c_2 & (-v_{2,n}+\mu_2 c_2)\mathrm{e}^{-\alpha_{2,n}a} \\ 0 & 0 & -\mathrm{e}^{-\alpha_{2,n}a} & 1 \end{pmatrix} \begin{pmatrix} A_{1,n} \\ B_{1,n} \\ A_{2,n} \\ B_{2,n} \end{pmatrix} = \begin{pmatrix} \sum_s C_{1,ns}\mathrm{e}^{-\alpha_{1,n}x_s} \\ \sum_s (-v_{1,n}+\mu_1 c_1)C_{1,ns}\mathrm{e}^{-\alpha_{1,n}(a-x_s)} + \sum_s -\mu_2 c_2 C_{2,ns}\mathrm{e}^{-\alpha_{2,n}x_s} \\ \sum_s \mu_1 c_1 C_{1,ns}\mathrm{e}^{-\alpha_{1,n}(a-x_s)} + \sum_s (v_{2,n}-\mu_2 c_2)C_{2,ns}\mathrm{e}^{-\alpha_{2,n}x_s} \\ \sum_s C_{2,ns}\mathrm{e}^{-\alpha_{2,n}(a-x_s)} \end{pmatrix}. \quad (36)$$

The above system fully determines the four constants for any n, the energy is then calculated at any point x, y by applying Eq. (26).

Eqs. (21) and (22) are solved with the collocation method. The boundary is discretized into N elements on which the unknown σ is assumed to be constant. The constant value is denoted $\sigma_{i,k}$ where the first subscript is related to the system i and the second is related to the element k. Eq. (21) is re-written as

$$\frac{1}{\pi}\sigma_{i,k} = \sum_s P_s \frac{\mathrm{e}^{-mR}}{2\pi R}\cos\varphi + \sum_l \sigma_{i,l}\int_{\Gamma_l} \cos\theta \frac{\mathrm{e}^{-mR'}}{2\pi R'}\cos\varphi \mathrm{d}\Gamma, \quad (37)$$

where R is the distance between the s^{th} force and the collocation point $\mathbf{p}_k$ chosen as the centre of the segment Γ_k, $R = |\mathbf{q} - \mathbf{p}_k|$, φ is the incidence angle at $\mathbf{p}_k$ and θ the emission angle at $\mathbf{q}$. In a similar manner, Eq. (22) at the interface of two sub-systems, becomes

$$\frac{1}{\pi}\sigma_{i,k} = \sum_{j,s} R_{ji}(\varphi) P_s \frac{\mathrm{e}^{-m_j R}}{2\pi R}\cos\varphi + \sum_{j,l} \sigma_{j,l}\int_{\Gamma_l} R_{ji}(\varphi)\cos\theta \frac{\mathrm{e}^{-m_j R'}}{2\pi R'}\cos\varphi \mathrm{d}\Gamma. \quad (38)$$

Finally, the vibrational energy at any point $\mathbf{r}$ inside sub-system i is calculated with the discretized form of Eq. (15),

$$W_i(\mathbf{r}) = \sum_s P_s \frac{\mathrm{e}^{-mR}}{2\pi cR} + \sum_k \sigma_{i,k}\int_{\Gamma_k} \cos\theta \frac{\mathrm{e}^{-mR'}}{2\pi cR'}\mathrm{d}\Gamma. \quad (39)$$

The integrals of Eqs. (37)-(39) are evaluated with a Gauss quadrature.

6 Numerical simulation

The numerical simulation is performed with the following characteristics. Both plates are made of steel, volumic mass $\rho = 7800$ kg/m^3, Young's modulus $E = 2.1\ 10^{11}$ N/m^2, Poisson's coefficient

	125 Hz	1 kHz	4 kHz	16 kHz
λ/h	150	53	26	13
a/λ	4	10	21	43
M	2.4	19	78	313

Table 1: Ratios λ/h, a/λ and modal overlap M ($\eta = 5\%$) versus frequency for plate 1.

	125 Hz	1 kHz	4 kHz	16 kHz
λ/h	89	31	16	8
a/λ	2	6	13	25
M	0.8	6	25	101

Table 2: Ratios λ/h, a/λ and modal overlap M ($\eta = 5\%$) versus frequency for plate 2.

$\nu = 0.3$, with same dimensions, length and width $a = b = 2$ m but with different thicknesses, $h_1 = 3.25$ mm for the first plate and $h_2 = 10$ mm for the second plate.

Plate 1 is excited by a transverse force of strenght $F = 1$ N located at $x_0 = 0.6$, $y_0 = 0.5$. The resulting injected power is given by the asymptotic formula $P = |F^2|/16\sqrt{D\rho h} = 4.83\,10^{-4}$ W, where $D = Eh^3/12(1-\nu^2)$ is the bending stiffness of the excited plate. Although this example has been chosen to highlight the difference between both energy methods, these plates may be encountered in ships or other large vehicles for which it is sometimes necessary to increase the damping loss factor by adding a damping material.

The wavelength is about 10 cm at 4 kHz for the thin plate and 16 cm for the thick plate. This is large enough compared with the thickness to apply Love plate equation. It is shown in Tables 1 and 2 that the ratio wavelength over thickness is larger than 8 for all the octave bands from 125 Hz up to 16 kHz. Compared with the size of plates, wavelength of flexural wave is short even for the thick plate at the lowest frequency. The values of the ratio length over wavelength are also summarized in Tables 1 and 2. It is then apparent that both plates vibrate at high frequencies over all the octave bands.

The reference calculation given in Appendix C is realized with 200 sine functions in Eq. (53) which is enough to predict the $200 \times 200 = 40000$ first modes of a square plate. The asymptotic modal densities of the plates are respectively 0.39 mode/Hz for the first plate and 0.13 mode/Hz for the second plate. The total number of modes in the bandwidth 88 Hz - 22600 Hz (8 octave bands) is approximately 11700. The solution for the vibrational conductivity is given by Eq. (26). The series is assessed with 200 cosine functions. Finally, the radiative energy transfer equations (37)-(39) are discretized with 1600 boundary elements which is very large to get an accurate response.

In Fig. 2 is shown the energy density at two points on each plate from 88 Hz to 22600 Hz for a damping loss factor $\eta = 5\%$. The positions are $x = 0.5$, $y = 0.5$ (points 1 and 3) and $x = 1.5, y = 1.5$ (points 2 and 4) in the local frames of Fig. 1. Results from vibrational conductivity and from radiative energy transfer have been computed at the frequencies 125 Hz, 250 Hz, 500 Hz, 1 kHz, 2 kHz, 4 kHz, 8 kHz and 16 kHz. Point 1 is located in the vicinity of the driving point and thus, the vibrational level is dominated by the direct field. However, it has ever been remarked in the literature [3, 24] that the energy of a cylindrical wave is poorly represented by a superposition of plane wave energies. This explains that the energy of direct field is under-estimated by vibrational

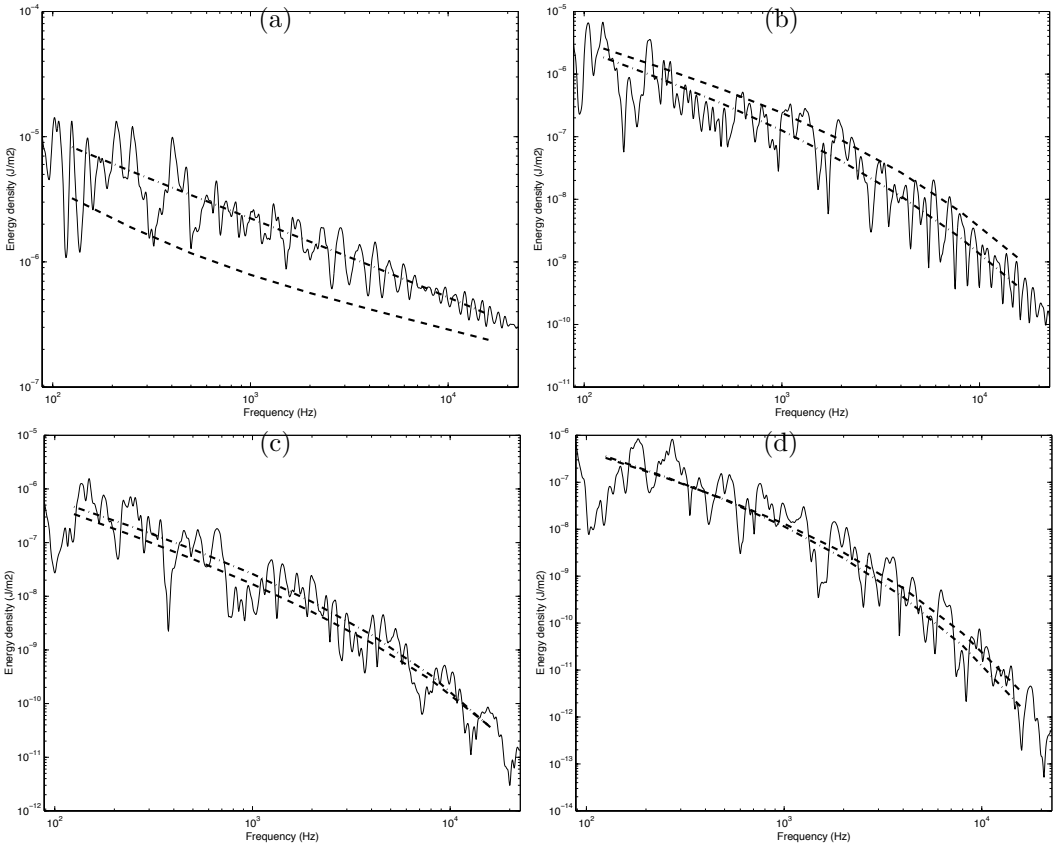

Figure 2: Vibrational energy versus frequency at (a), point 1, (b), point 2, (c), point 3 and (d), point 4 for $\eta = 5\%$: (—), reference calculation; (- -), vibrational conductivity; (-.-), radiative energy transfer.

conductivity. Furthermore, both energy methods verify the global power balance (Eqs. (2) and (20)). For a same amount of injected power, the total vibrational energy predicted by vibrational conductivity and radiative energy transfer, is the same. An under-estimation of energy in the direct field then leads to an over-estimation of energy in far-field (points 2, 3 and 4).

In Figs. 3-5 is shown the vibrational energy density contained in the octave band centred in 4000 Hz along the x-axis for three values of damping loss factor ($\eta = 10\%$, $\eta = 5\%$ and $\eta = 1\%$). In case (a) the line $y = 0.5$ m passes near the excitation point and in case (b) the line $y = 0.98$ m is almost centred in the pair of plates. The direct field is particularly clear in the case $\eta = 10\%$ (Fig. 3). The decrease of the energy density like e^{-mr}/r where r is the source-receiver distance is well predicted by the radiative energy transfer whereas vibrational conductivity leads to the law $\mathrm{e}^{-mr}/\sqrt{r}$. A lack of 1.5 dB per doubling distance is attributable to the last law. In the second plate, the energy seems to be correctly predicted by both methods. However, a careful observation of the results reveals that if the mean energy is the same for both methods, the repartition of energy is not. For instance, the case of light damping (Fig. 5) shows that vibrational conductivity does not predict any variation in the energy field whereas radiative energy transfer predicts 2 dB difference from left to right. When the damping loss factor goes to zero, (Figs. 4 and 5) vibrational conductivity and radiative energy transfer converge to SEA. It is then apparent that vibrational

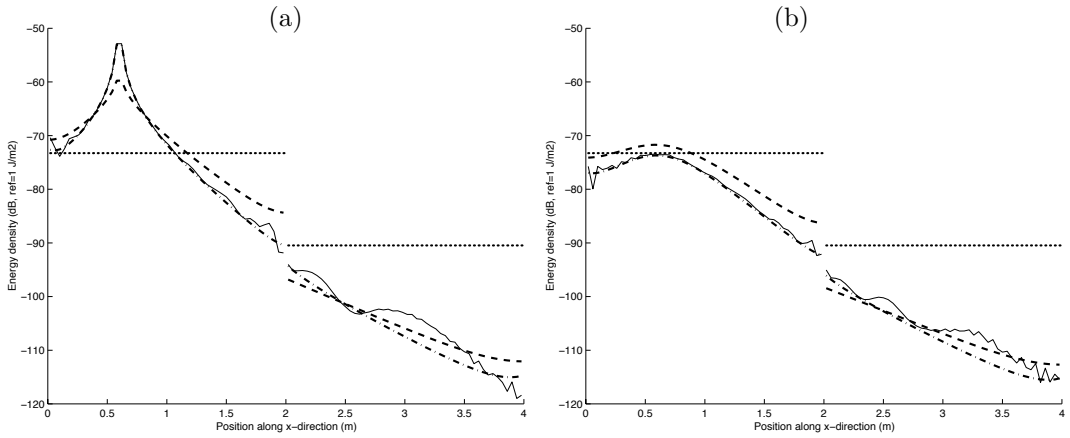

Figure 3: Wideband vibrational energy (octave 4000 Hz) versus position for $\eta = 10\%$. Case (a), $y = 0.5$ m and case (b), $y = 0.98$ m. (—), reference calculation; (...), SEA; (- -), vibrational conductivity; (-.-), radiative energy transfer.

conductivity applies for slightly damped structures.

7 Conclusion

In this paper, two methods intended for the prediction of wideband vibrational levels have been compared. Both methods were developped to extend the validity domain of SEA, and, in particular, to predict the repartition of energy inside sub-structures. Indeed, this gain of information requires more computation than SEA, but yet significantly less than classical FEM which can predict pure tone vibrational levels. These methods are thus midway between classical FEM and SEA. The vibrational conductivity is based on an analogy with conduction in heat transfer whereas the radiative energy transfer approach is based on an analogy with radiative heat transfer. The former assumes that the vibrational field is a superposition of plane waves, that is the field is diffuse or slightly non diffuse. The latter assumes that the energy propagates as rays and then applies for wider class of fields under the condition that the wavelength is short. Radiative energy transfer leads to some integral equations solved with conventional numerical schemes of BEM. Vibrational conductivity leads to a differential equation which can be solved with FEM, more widely spread than BEM. This is probably an important argument to explain the increasing popularity of vibrational conductivity.

Acknowledgments

The author gratefuly acknowledges Professor M. Moussaoui for his kind and efficient advice.

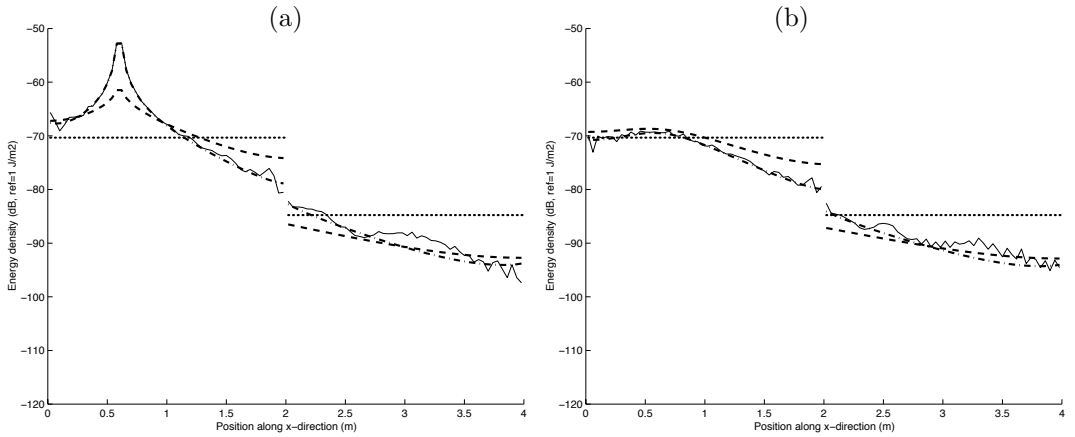

Figure 4: Wideband vibrational energy (octave 4000 Hz) versus position for $\eta = 5\%$. Case (a), $y = 0.5$ m and case (b), $y = 0.98$ m. (—), reference calculation; (...), SEA; (- -), vibrational conductivity; (-.-), radiative energy transfer.

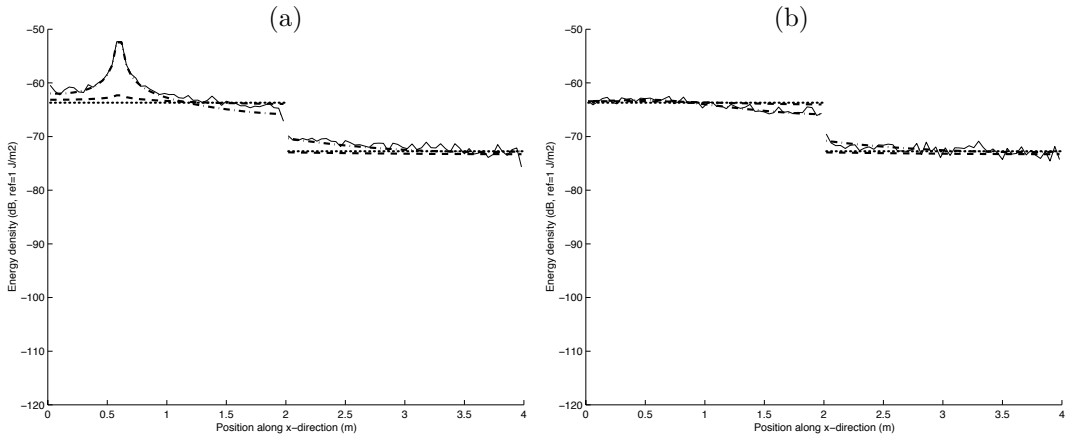

Figure 5: Wideband vibrational energy (octave 4000 Hz) versus position for $\eta = 1\%$. Case (a), $y = 0.5$ m and case (b), $y = 0.98$ m. (—), reference calculation; (...), SEA; (- -), vibrational conductivity; (-.-), radiative energy transfer.

Appendix A

In this Appendix, it is found that the energy field given in Eq. (15) results from the boundary integral solution of Love plate equation.

Consider the solution of Eq. (52),

$$v(\mathbf{r}) = \sum_k F_k g(\mathbf{s}_k, \mathbf{r}) + \int_\Gamma \frac{\partial \triangle g}{\partial n} v - \triangle g \frac{\partial v}{\partial n} + \frac{\partial g}{\partial n} \triangle v - g \frac{\partial \triangle v}{\partial n} \mathrm{d}\Gamma, \tag{40}$$

where in the integral g (and its derivatives) is taken as $g(\mathbf{p}, \mathbf{r})$ and v is $v(\mathbf{p})$. $\mathbf{n}$ is the outward unit normal to the boundary at point $\mathbf{p}$ and g is the standard Green function for infinite plates, *i.e.* $g(\mathbf{p}, \mathbf{r}) = \mathrm{i}[\mathrm{H}_0^{(2)}(kR) - \mathrm{H}_0^{(2)}(\mathrm{i}kR)]/8k^2$ (convention $\mathrm{e}^{i\omega t}$) where $R = |\mathbf{p} - \mathbf{r}|$ and $k = k_0(1 - \mathrm{i}\eta/4)$ is the complex wavenumber of the plate and $\mathrm{H}_0^{(2)}$ is the Hankel function of second kind and order zero. The energy field is obtained by squaring the modulus of the response.

$$W(\mathbf{r}) = \frac{1}{2}\rho\omega^2 |v(\mathbf{r})|^2, \tag{41}$$

where ρ is the mass per unit area. Now, all forces F_k and responses $v(\mathbf{p})$ (and its derivatives) are assumed to be δ-correlated random variables. The correlations are,

$$< F_k \, F_l^* >=< F_k \, F_k^* > \delta_{kl}, \tag{42}$$

$$< F_k \, \mathrm{L}_i v^*(\mathbf{p}) >= 0, \tag{43}$$

$$< \mathrm{L}_i v(\mathbf{p}) \, \mathrm{L}_j v^*(\mathbf{p}') >=< \mathrm{L}_i v(\mathbf{p}) \, \mathrm{L}_j v^*(\mathbf{p}) > \delta(\mathbf{p} - \mathbf{p}'), \tag{44}$$

where $\mathrm{L}_i = 1$, $\partial./\partial n$, $\triangle.$, $\partial \triangle ./\partial n$ for $i = 0$, ... 4. This assumption ensures that all interferences have been neglected. So, the expected value of energy is,

$$< W >= \frac{1}{2}\rho\omega^2 \left(\sum_k < F_k \, F_k^* > |g|^2 + \sum_{i,j} \int_\Gamma (-1)^{i+j} \mathrm{L}_i g \, \mathrm{L}_j g^* < \mathrm{L}_{4-i} v \, \mathrm{L}_{4-j} v^* > \mathrm{d}\Gamma \right). \tag{45}$$

The sixteen functions $\mathrm{L}_i g \, \mathrm{L}_j g^*$ can be evaluated from the expression for the Green's function. In far-field, the asymptotic expansions are,

$$g = \frac{\mathrm{i}}{8k^2} \mathrm{e}^{\mathrm{i}\pi/4} \sqrt{\frac{2}{\pi k R}} \mathrm{e}^{-\mathrm{i}kR}, \tag{46}$$

$$\frac{\partial g}{\partial n} = \frac{1}{8k} \cos\theta \mathrm{e}^{\mathrm{i}\pi/4} \sqrt{\frac{2}{\pi k R}} \mathrm{e}^{-\mathrm{i}kR}, \tag{47}$$

$$\triangle g = -\frac{\mathrm{i}}{8} \mathrm{e}^{\mathrm{i}\pi/4} \sqrt{\frac{2}{\pi k R}} \mathrm{e}^{-\mathrm{i}kR}, \tag{48}$$

$$\frac{\partial \triangle g}{\partial n} = -\frac{k}{8} \cos\theta \mathrm{e}^{\mathrm{i}\pi/4} \sqrt{\frac{2}{\pi k R}} \mathrm{e}^{-\mathrm{i}kR}, \tag{49}$$

where θ is the emanating angle at $\mathbf{p}$. It is now apparent that,

$$\mathrm{L}_i g \, \mathrm{L}_j g^* \propto \frac{\mathrm{e}^{-mR}}{2\pi R}, \tag{50}$$

where $m = \eta k_0/2$ for any i, j. Finally,

$$< W >= \sum_k P_k \frac{\mathrm{e}^{-mR}}{2\pi cR} + \int_\Gamma \sigma(\mathbf{p}, \theta) \frac{\mathrm{e}^{-mR}}{2\pi cR} \mathrm{d}\Gamma, \tag{51}$$

where $P_k = \rho\omega^3 < F_k\, F_k^* > /32k^6$ and σ is an unknown function (since v is *a priori* not known on the boundary Γ) depending on the position $\mathbf{p}$ (through v and its derivatives) and the emanating angle θ.

It is remarkable that in Eq. (51) all terms collapse in a single scalar function. It means that, under the far-field assumption, monopoles, dipoles and other multipoles up to the order 4 radiate energy following a $\mathrm{e}^{-mR}/2\pi R$ law. The only difference between these sources is the directivity function which,indeed, is quite different.

Appendix B

It is proved here that the energy field given in Eq. (15) cannot verify a linear differential equation. Homegeneity implies that the differential operator has constant coefficients and isotropy implies that it is elliptic. Consider the case $m = 0$ and $\Omega = B(0, 1)$ the unit open ball centred in the origin in dimension 2. If it exists an elliptic differential operator P of order l such that $Pu = \delta$ then $u \in \mathrm{H}^{-2+l}(\Omega)$ where $\mathrm{H}^s(\Omega)$ is the Sobolev's space. The case $l \leq 2$ can be discarded by a direct calculation since isotropy implies that $P = a\mathrm{Id} + b\triangle$. and $1/r$ cannot be the fundamental solution. Then we can assume $l \geq 3$ and thus, $u \in \mathrm{H}^{-2+l} \subset \mathrm{H}^1$ but $1/r \notin \mathrm{H}^1$. This proves that $1/r$ cannot be the fundamental solution of any elliptic operator of any order in dimension 2.

Appendix C

The reference calculation is considered in this Appendix. The Love equation for plates is

$$\Delta^2 v - k^4 v = \frac{1}{D} \sum_s F_s \delta(x - x_s)\delta(y - y_s), \tag{52}$$

where v is the transverse deflection, D is the bending stiffness and k the wavenumber. The deflection v is developped as a Fourier series,

$$v(x, y) = \sum_{n=1}^{\infty} v_n(x) \sin(\frac{n\pi y}{b}), \tag{53}$$

where the cosine terms are discarded since the simply supported condition imposes $v = \partial^2 v/\partial y^2 + \nu\partial^2 v/\partial x^2 = 0$ at $y = 0$ and $y = b$. Subtitution of Eq. (53) into Eq. (52) leads to,

$$\frac{\mathrm{d}^4 v_n}{\mathrm{d}x^4} - 2\left(\frac{n\pi}{b}\right)^2 \frac{\mathrm{d}^2 v_n}{\mathrm{d}x^2} - \left[k^4 - (\frac{n\pi}{b})^4\right] v_n = \frac{2}{Db} \sum_s F_s \sin(\frac{n\pi y_s}{b})\delta(x - x_s), \tag{54}$$

with the solution,

$$\begin{aligned} v_n(x) \quad = \quad & A_n \mathrm{e}^{-\mathrm{i}\beta_n x} + B_n \mathrm{e}^{-\mathrm{i}\beta_n (a-x)} + C_n \mathrm{e}^{-\mathrm{i}\gamma_n x} + D_n \mathrm{e}^{-\mathrm{i}\gamma_n (a-x)} + \\ & \textstyle\sum_s E_{ns} \mathrm{e}^{-\mathrm{i}\beta_n |x_s - x|} + F_{ns} \mathrm{e}^{-\mathrm{i}\gamma_n |x_s - x|}, \end{aligned} \tag{55}$$

where β_n, $-\beta_n$, γ_n, $-\gamma_n$ are the four roots of the characteristic equation,

$$X^4 + 2\left(\frac{n\pi}{b}\right)^2 X^2 - \left[k^4 - (\frac{n\pi}{b})^4\right] = 0. \tag{56}$$

The constants E_{ns} and F_{ns} are determined by applying the continuity of $\mathrm{d}^2v_n/\mathrm{d}x^2$ *i.e.* $E_{ns}\beta_n + F_{ns}\gamma_n = 0$ and the condition $\mathrm{i}E_{ns}\beta_n^3 + \mathrm{i}F_{ns}\gamma_n^3 = 2F_s/bD \times \sin(n\pi y_s/b)$. The constants $A_{i,n}$, $B_{i,n}$, $C_{i,n}$ and $D_{i,n}$ of plates $i = 1, 2$ are finally determined by applying the boundary conditions for simply supported edges,

$$\begin{aligned}
v_{1,n}(0) &= 0, & (57)\\
\frac{\partial^2 v_{1,n}}{\partial x^2}(0) + \nu\frac{\partial^2 v_{1,n}}{\partial y^2}(0) &= 0, & (58)\\
v_{2,n}(a) &= 0, & (59)\\
\frac{\partial^2 v_{2,n}}{\partial x^2}(a) + \nu\frac{\partial^2 v_{2,n}}{\partial y^2}(a) &= 0, & (60)
\end{aligned}$$

and the continuity conditions at the interface,

$$\begin{aligned}
v_{1,n}(a) &= v_{2,n}(0), & (61)\\
\frac{\partial v_{1,n}}{\partial x}(a) &= \frac{\partial v_{2,n}}{\partial x}(0), & (62)\\
\frac{\partial^2 v_{1,n}}{\partial x^2}(a) + \nu\frac{\partial^2 v_{1,n}}{\partial y^2}(a) &= \frac{\partial^2 v_{2,n}}{\partial x^2}(0) + \nu\frac{\partial^2 v_{2,n}}{\partial y^2}(0), & (63)\\
\frac{\partial^3 v_{1,n}}{\partial x^3}(a) + (2-\nu)\frac{\partial^3 v_{1,n}}{\partial x\partial y^2}(a) &= \frac{\partial^3 v_{2,n}}{\partial x^3}(0) + (2-\nu)\frac{\partial^3 v_{2,n}}{\partial x\partial y^2}(0), & (64)
\end{aligned}$$

leading to a system of eight linear equations.

Finally, the energy density density at any point is given by,

$$W(x,y) = \frac{\rho\omega^2}{4}|v|^2 + \frac{D}{4}\left[|\frac{\partial^2 v}{\partial x^2}|^2 + |\frac{\partial^2 v}{\partial y^2}|^2 + 2\nu\mathrm{Re}\left(\frac{\partial^2 v}{\partial x^2}\frac{\partial^2 v^*}{\partial y^2}\right) + 2(1-\nu)|\frac{\partial^2 v}{\partial x\partial y}|^2\right], \tag{65}$$

where Re designates the real value, * the complex conjugate and ρ the mass per unit area.

References

[1] D.J. Nefske and S.H. Sung. Power flow finite element analysis of dynamic systems: Basic theory and application to beams. *NCA Publication*, 3, 1987.

[2] J.C. Wohlever and R.J. Bernhard. Mechanical energy flow models of rods and beams. *Journal of Sound and Vibration*, 153:1–19, 1992.

[3] R.S. Langley. On the vibrational conductivity approach to high frequency dynamics for two-dimensional structural components. *Journal of Sound and Vibration*, 182:637–657, 1995.

[4] M. Djimadoum and J.L. Guyader. Possibilities to generalize the heat transfer approach to vibration of plates problems. In *Inter-Noise'95, Newport Beach CA*, 1995.

[5] P.E. Cho and R.J. Bernhard. Energy flow analysis of coupled beams. *Journal of Sound and Vibration*, 211(4):593–605, 1998.

[6] O.M. Bouthier and R.J. Bernhard. Simple models of energy flow in vibrating membranes. *Journal of Sound and Vibration*, 182(1):129–147, 1995.

[7] O.M. Bouthier and R.J. Bernhard. Simple models of energy flow in vibrating plates. *Journal of Sound and Vibration*, 182(1):149–164, 1995.

[8] D.H. Park and S.Y. Hong. Power flow models and analysis of in-plane waves in finite coupled thin plates. *Journal of Sound and Vibration*, 244(4):651–668, 2001.

[9] R.J. Bernhard and J.E. Huff. Structural-acoustics design at high frequency using the energy finite element method. *Journal of Vibration and Acoustics*, 121:295–301, 1999.

[10] Kuttruff H. Simulierte nachhallkurven in rechteckräumen mit diffusem schallfeld. *Acoustica*, 25:333–342, 1971.

[11] Carroll M.M. and Chien C.F. Decay of reverberent sound in a spherical enclosure. *Journal of Acoustical Society of America*, 62(6):1442–1446, 1977.

[12] Miles R.N. Sound field in a rectangular enclosure with diffusely reflecting boundaries. *Journal of Sound and Vibration*, 92(2):203–226, 1984.

[13] Kuttruff H. A simple iteration scheme for the computation of decay constants in enclosures with diffusely reflecting boundaries. *Journal of Acoustical Society of America*, 98(1):288–293, 1995.

[14] Franzoni L.P., Bliss D.B., and Rouse J.W. An acoustic boundary element method based on energy and intensity variables for prediction of high-frequency broadband sound fields. *Journal of Acoustical Society of America*, 110(6):3071–3080, 2001.

[15] A. Le Bot and L. Ricol. Integral equation instead of heat conduction equation for medium and high frequencies. In *Inter-Noise 95, Newport Beach USA*, pages 579–582, 1995.

[16] A. Le Bot. A vibroacoustic model for high frequency analysis. *Journal of Sound and Vibration*, 211(4):537–554, 1998.

[17] A. Le Bot. Energy transfer for high frequencies in built-up structures. *Journal of Sound and Vibration*, 250(2):247–275, 2002.

[18] E. Sarradj. High frequency boundary integral method as an alternative to statistical energy analysis. In *10th ICSV, Stockholm Sweden*, 2003.

[19] V. Cotoni, A. Le Bot, and L. Jezequel. High frequency radiation of L-shaped plate by a local energy flow approach. *Journal of Sound and Vibration*, 250(3):431–444, 2002.

[20] R.H. Lyon. *Statistical Energy Analysis of Dynamical Systems: Theory and Application*. Cambridge, Massachusetts, MIT Press, 1975.

[21] Beckmann Th. Wöhle W. and Schreckenbach H. Coupling loss factors for statistical energy analysis of sound transmission at rectangular slab joints, part. I. *Journal of Sound and Vibration*, 77(3):323–334, 1981.

[22] A. Le Bot. A functional equation for the specular reflection of rays. *Journal of Acoustical Society of America*, 112(4), 2002.

[23] W.B. Joyce. Sabine's reverberation time and ergodic auditoriums. *Journal of Acoustical Society of America*, 58(3):643–655, 1975.

[24] A. Le Bot. Geometric diffusion of vibrational energy and comparison with the vibrational conductivity approach. *Journal of Sound and Vibration*, 212(4):637–647, 1998.